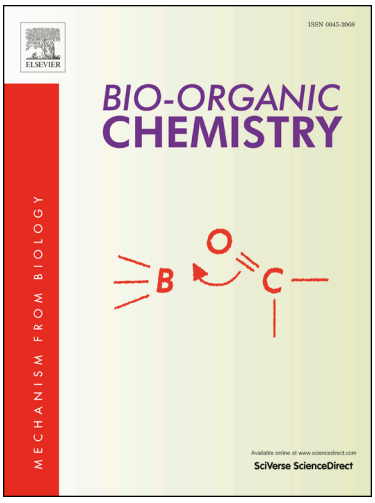

Molecular dynamics guided development of indole based dual inhibitors of EGFR (T790M) and c-MET

Pankaj Kumar Singh, Om Silakari

PII: S0045-2068(18)30198-6
DOI: https://doi.org/10.1016/j.bioorg.2018.04.001
Reference: YBIOO 2324

To appear in: *Bioorganic Chemistry*

Received Date: 2 March 2018
Revised Date: 4 April 2018
Accepted Date: 6 April 2018

Please cite this article as: P. Kumar Singh, O. Silakari, Molecular dynamics guided development of indole based dual inhibitors of EGFR (T790M) and c-MET, *Bioorganic Chemistry* (2018), doi: https://doi.org/10.1016/j.bioorg.2018.04.001

Molecular dynamics guided development of indole based dual inhibitors of EGFR (T790M) and c-MET

Pankaj Kumar Singh, Om Silakari*

Molecular Modelling Lab (MML), Department of Pharmaceutical Sciences and Drug research,

Punjabi University, Patiala, Punjab, 147002, India

**Corresponding authors E-mail: omsilakari@gmail.com; Tel: +91-9501542696; Fax: +91-1752283075*

Abstract

Secondary acquired mutation in EGFR, *i.e*. EGFR T790M and amplification of c-MET form the two key components of resistant NSCLC. Thus, previously published pharmacophore models of EGFR T790M and c-MET were utilized to screen an *in-house* database. On the basis of fitness score, indole-pyrimidine scaffold was selected for further evaluation. Derivatives of indole-pyrimidine scaffold with variedly substituted aryl substitutions were sketched and then docked in both the targets. These docked complexes were then subjected to molecular dynamic simulations, to study the stability of the complexes and evaluate orientations of the designed molecules in the catalytic domain of the selected kinases. Afterwards, the complexes were subjected to MM-GBSA calculation, to study the effect of substitutions on binding affinity of double mutant EGFR towards these small molecules. Finally, the designed molecules were synthesized and evaluated for their inhibitory potential against both the kinases using *in-vitro* experiments. Additionally, the compounds were also evaluated against EGFR (L858R) to determine their selectivity towards double mutant, resistant kinase [EGFR (T790M)]. Compound **7a** and **7c** were found to be possess nanomolar range inhibitory (IC_{50}) potential against EGFR (T790M), **7h** showed good inhibitory potential against c-MET with IC_{50} value of 0.101 µM. Overall, this work is one of the earliest report of compounds having significant dual inhibitory potential against secondary acquired EGFR and cMET, with IC_{50} values in nanomolar range.

Keywords: Indole-pyrimidine; molecular dynamic simulations; EGFR (T790M); c-MET

1. Introduction

Kinases form a major class of molecular targets in lung adenocarcinomas harbouring activating mutations. These kinases result in over-activation of downstream signalling pathways that regulate the process of cell growth, proliferation, and survival. The identification of these driver kinases has previously led to the clinical use of small molecule kinase inhibitors such as erlotinib and gefinitib [1, 2]. These molecules act as competitive inhibitors of ATP and have been proven efficacious over conventional chemotherapies in patients harbouring epithelial growth factor receptor (EGFR) overexpressed adenocarcinomas [3]. However, clinical responsive success of these kinase targeted inhibitors has been observed to be short lived due to development of acquired resistance to these drugs. Multiple mechanisms have been identified as the cause for the failure of these molecules which include: (1) alteration in the driver oncogene such as acquired secondary mutation T790M in EGFR (2) activation of signaling pathway(s) *via* parallel signalling, as in case of amplification of wildtype c-MET (hepatocyte growth factor receptor) in the L858R mutant EGFR overexpressed lung cancer and (3) reactivation of signalling pathways downstream of a driver oncogene, Nuclear factor-κB (NFκB)-containing complex activation is one such example. One more mechanism of resistance involves transformation of cell lineage such as epithelial (Non-small cell lung cancer) to another *i.e.*, mesenchymal (Small cell lung cancer) [4].

Among all, secondary acquired gate keeper residue mutation, T790M in EGFR, is observed in ~50% of EGFR-mutant patients who develop resistance to EGFR inhibition and is a pivotal mechanism of resistance. Initially, researchers suggested that gatekeeper mutation results in steric hindrance towards small molecule inhibitors thereby leading to development of resistance [5]. Later, studies disclosed that secondary acquired kinase do not possess resistance due to steric hindrance but rather the affinity of the kinase is altered back in favour of ATP and hence, ATP competitively inhibits the inhibitors [6]. To counter this secondary acquired mutation, researchers focussed on developing second generation kinase inhibitors, covalent inhibitors. Several studies focused on developing covalent inhibitors for EGFR T790M, via analysis of catalytic mechanism of binding with Cys797 [7] and utilization of different cysteine-trapping fragments [8] such as isothiocyanates [9], have been conducted. However, they suffer with lack of selectivity and therefore have poor safety profile. This further led to the development of third generation kinase inhibitors, which are covalent but are selective towards double mutant EGFR. Selectivity in these agents is claimed due to the hydrophobic interactions between the inhibitors and mutated residue M790 in the catalytic

domain of the double mutant kinase. Osimertinib, recently reported EGFR (T790M) inhibitor, was also based on the same concept that molecules with hydrophobic interaction with the mutant methionine-790 gatekeeper residue could result in potent and selective inhibitors. It is also potent inhibitor of EGFR (L858R) due to its increased affinity towards small molecule inhibitors in place of ATP [10]. However, as covalent inhibitors are site specific in nature, any alteration in target residues can limit their efficacy. In recent years another acquired mutation, C797S in EGFR, has been disclosed and reported to make third generation inhibitors ineffective. Additionally, another mutation in the P-loop residue (L718Q) has been reported to result in resistance against third generation inhibitors such as osimertinib. One of the mechanism suggests that mutant Gln718 affects the conformational space of the EGFR–osimertinib complex, preventing its interaction with Cys797 [11].

Another key mechanism of resistance against kinase inhibitors in NSCLC (Non-small cell lung cancer) is amplification of c-MET, upon administration of first generation inhibitors. It has been one of the earliest mechanism of resistance which rendered EGFR inhibitors ineffective [12]. Amplification of c-MET leads to the reactivation of PI3K/Akt signaling pathway by forming a MET-ErbB-3 heterodimer, previously formed by EGFR. Basically, c-MET behaves as a substitute for EGFR in the signalling pathway. Thus, despite continuous suppression of EGFR by the inhibitor, a critical downstream signalling pathway continues, and resistance to the inhibitor emerges [13]. In patients with resistance to first-generation EGFR tyrosine kinase inhibitors generated by c-MET amplification, it is unlikely that a third generation covalent inhibitor would be effective, but the combination of a double mutant EGFR inhibitor and a c-MET/mTOR/ PI3K/Akt pathway inhibitor may prove to be an effective strategy [14]. Clinical trials are underway to test the effect of dual inhibition of c-MET and EGFR to overcome this mode of resistance [15].

Thus, in our study we focussed on targeting c-MET and secondary acquired mutant EGFR (T790M) via non-covalent inhibitors. Focus was laid on the fact that sensitivity towards inhibitors is not lost in T790M EGFR rather the affinity towards ATP increases. Special attention was also given to the fact that molecules having hydrophobic interaction with mutant residue M790 provide selectivity to the molecules and thus, may also enhance the binding affinity towards EGFR T790M. Thus, we attempted to design molecules with higher affinity towards T790M EGFR along with c-MET using *in-silico* techniques and further synthesis and biological evaluation.

2. Results and Discussion

2.1.*In-silico* analysis

.Previously reported ligand-based pharmacophore models for EGFR (T790M) and cMET, generated using Discovery studio were employed to screen and cross screen an *in-house* small molecule database containing around 200 molecules with diverse scaffolds such as benzimidazole, oxindole, indole, flavones and thiazolidinones. Pharmacophore mapping tool was employed for this purpose and molecules possessing significant fit score in mapping via both pharmacophores were selected for further analysis. This screening yielded a total of 18 molecules with indole scaffold, similar compounds have been reported previously to possess anti-microbial and cytotoxic potential [16-18], which were then subjected to docking analysis using co-crystallized 3-D structure of both the target kinases followed by molecular dynamic simulations and calculation of MM-GBSA score (binding energies). For molecular docking, the PDB were selected utilizing resolution as cut-off followed by cross docking protocol (**supplementary table s1, s2, s3 and s4**). Molecules selected after docking analysis, in EGFR T790M, showed that an amino group present at the second position of the pyrimidine containing molecules acts as donor group and interacts *via* hydrogen bond with Gln791, Met793 and Lys745 in many of the designed compounds while the ring of indole formed the hydrophobic interactions with various other hinge region residues. Similarly, in cMET, free NH_2 in many of the designed compounds formed hydrogen bond with Asp1231 and the hydrophobic region was occupied by benzyl group substituted at N^1 of the indole. All the compounds showed good docking scores (Glide XP G-score) in both the kinases; ranging from -8.22 to -6.98 kcal/mol within the EGFR (T790M) protein and -7.42 to -4.59 kcal/mol in cMET. Docking was followed by molecular dynamic simulations of the designed molecules in complex with EGFR (T790M) as well as cMET, for a period of 30 ns. Simulations studies disclosed that almost all the molecules were maintaining key H-bond interactions with hinge region amino acids. A key disclosure was the fact that nine molecules were maintaining varied levels of hydrophobic interactions with mutated gate keeper residue M790 which is essential for the selectivity and potency of molecules against double mutant EGFR (T790M), which were then forwarded for synthesis and in-vitro evaluation. Additionally, presence of bromine in the side ring was found to be vital as it occupied small hydrophobic cavity in the catalytic domain of EGFR (T790M) enhancing the overall hydrophobic and van der waal interactions, while in some derivatives it also formed halogen bond with neighbouring residues. The RMSD values of the protein and ligands in the complex with top compounds (**7c** and **7h)** reflected the overall stability of the complex for the given period of 30 ns and the graphs for the same are represented in **Fig.1** and **Fig.2**.

<figure1>

<figure2>

The 3D interaction diagram of the designed molecules **7c** in EGFR T790M and **7h** in cMET are shown in **fig.3** and **fig.4**, respectively. Finally binding energy scores, calculated using MM-GBSA protocol, reflected significant affinity for the designed molecules in both the targets. The score of all the compounds lied in the range of -75.706 to -49.003 in EGFR (T790M) and -84.334 to -66.319 in cMET (**Table 1**).

<figure3>

<figure4>

<table1>

2.2.Chemistry

The designed compounds were synthesized according to the **scheme 1**. In the first step, alkylation of indole-3-carbaldehyde was performed by reacting it with variedly substituted benzyl chlorides in the presence potassium carbonate to yield different N-substituted indole-3-carbaldehydes. Followed by claisen-schmidt condensation of the obtained N-substituted indole-3-carbaldehydes with *p*-bromoacetophenone using piperidine as catalyst in methanol to afford 1,3-diaryl/heteroaryl propenones. The obtained 1,3-diaryl propenones were purified via recrystallization. Then, 1,3-diaryl/heteroaryl propanones were treated with guanidine hydrochloride, using sodium hydroxide as catalyst in methanol to afford desired products. Finally column chromatography was performed to obtain pure derivatives. All the compounds were characterized by IR, Mass, ^{1}H-NMR and ^{13}C-NMR. In IR spectrum, the indole-pyrimidine derivatives showed the presence of strong absorption bands of multiple C=N from ~1680 to ~1580 cm^{-1}. The synthesis of final compounds were confirmed in ^{1}H-NMR. Almost each spectrum showed singlet of only proton present in pyrimidine nucleus, ranging from ~7.3 to ~7.8 ppm according to different derivatives. Rest of the aromatic protons were observed in a similar pattern from ~7.0 to ~ 8.4 ppm. A singlet of two proton at ~5.5 ppm was also observed in each spectrum for -CH_2 of the benzyl groups. ^{13}C spectrum exhibited characteristic peaks at ~163 ppm for pyrimidines. Rest of the aromatic carbons were observed from 120 to 134 ppm with a characteristic peak at 55 ppm for benzylic carbon. Similarly, mass spectrometry also showed quasi ion peaks at expected *m/z* values,

additionally, an M+2 peak was observed in each case due to presence of -Br group in each molecule.

<scheme1>

2.3.*In-vitro* biological evaluation

For the *in vitro* evaluation of kinase inhibitory potential of the synthesized compounds, enzymatic assay against EGFR (T790M) and cMET were performed. Additionally evaluation against EGFR (L858R) was also performed, which is involved in development of NSCLC in around 50 % patients on the first place. Appropriate standard (i.e. erlotinib), controls and test samples were utilized. The test compounds were used at the concentration of 0.1, 1 and 10 µM, and inhibitory potential was characterized by IC_{50} value. Compound **7a** with ethyl substitution at para position of benzyl attached to indole was found to possess significant selective EGFR (T790M) inhibitory activity over EGFR (L858R) with IC_{50} value 0.097 µM in EGFR (T790M) and 0.913 µM in EGFR (L858R). It also showed significant cMET inhibitory potential with IC_{50} value 0.518 µM. Another compound **7c** having 4-isopropyl substituted benzyl substitution showed excellent non-selective inhibition in both EGFR (T790M) and EGFR (L858R) with IC_{50} values 0.094 and 0.099 µM, respectively. Additionally it also showed modest cMET inhibitory activity with IC_{50} value 0.595. However, upon substituting isopropyl with isobutyl the inhibitory activity in compound **7b** fell to IC_{50} value 0.569 µM. Compound **7h** with 3-chloro substitution was found to be most potent cMET inhibitor with IC_{50} value 0.101 µM as summarized in **Table 2**. The inhibitory potential against EGFR (T790M) can be correlated with hydrophobic interactions between mutated residue M790 and bulk of the substituent group at N-benzyl group. Isopropyl substituent was found to be most optimum for significant inhibitory potential.

<table2>

3. Conclusion

Acquired secondary mutation T790M in EGFR and amplification of cMET are two most important resistance mechanisms hampering chemotherapy in NSCLC. Therefore, in this study *in-silico* methodologies were employed to design some indole-pyrimidine scaffold based reversible dual inhibitors of EGFR (T790M) and cMET. The designed compounds were further synthesized and evaluated for their kinase inhibitory potential using enzymatic

assay. Compound **7a, 7c** and **7h** showed significant dual inhibitory potential against both EGFR (T790M) and cMET. This work is one of the earliest reports for molecules with dual inhibitory potential against double mutant EGFR and cMET. The obtained results lay ground for further efforts to develop small molecule dual inhibitors of EGFR T790M-cMET for resistant NSCLC.

4. Material and methods

4.1.*In-silico* study

Previously published pharmacophore models for EGFR (T790M) and c-MET [19] were utilized to screen an *in-house* database of synthetically feasible compounds via pharmacophore mapping tool available with Discovery studio software [20]. After screening, molecules with good fitness score, close to score of active molecules in the training set of pharmacophores, were subjected to structure based drug designing techniques such as molecular docking. The docking studies were carried out using Glide module of Schrödinger [21]. The screened molecules were first docked into the grid of PDB ID: 2W2P for EGFR (T790M) followed by docking into the grid of 3DKF for c-MET and vice-versa, using extra precision (XP) docking module, which predicts the binding modes and their Glide XP G-score. Generated docking poses were then analysed based on the conserved molecular interactions reported mandatory to possess significant inhibitory potential in both the kinases. Along with hydrogen bonds between the ligand and the active site residues Met793, Lys745 and others, molecules were analysed for hydrophobic interaction with the mutant residue M790 in EGFR (T790M). While, in c-MET, poses having interactions with Met1160 and other residues in the hinge region of the active site were selected.

To check the stability of the designed molecules in the catalytic domain of both T790M EGFR and c-MET, the docked complexes were subjected to molecular dynamics (MD) simulations for a time period of 30 ns. The MD simulations were carried out with OPLS_2005 force field in Desmond software of Schrödinger [22]. An octahedral water box of 1 nm thickness was generated and solvated using a TIP3P water model. At physiological pH, protein-ligand complexes were charged accordingly, the system was neutralized by adding counter-ions and salt concentration was fixed to 0.15 M. After the energy minimization, the NPT equilibration was conducted at 310 K. A Nose-Hoover chain method thermostat was used to maintain constant temperature. NVT was followed by NPT equilibration applied at a pressure of 1 bar, maintained by a Martyn-Tobias-Klein barostat. During equilibration, the protein backbone was restrained and the solvent, molecules along

with counter-ions were allowed to move. The MD simulations were performed under periodic boundary conditions to avoid edge effects. The simulations were conducted with a time step of 1 fs and the coordinate data were stored in the file. The trajectory potentials were obtained from each MD simulation. RMSD value was calculated using 'simulation event analysis' protocol of Desmond for each T790M EGFR and c-MET complex. The binding orientations of the ligand within the protein were studied using a simulation interaction diagram. Finally, the binding energies of the molecules with both the target kinases were calculated using Prime MM-GBSA module. This methodology calculates the binding energy of ligand with the receptor as the sum of gas-phase internal energy, estimated using a molecular mechanics force field, and the solvation free energy, calculated using an implicit solvent model (Generalized Born Surface Area). Additionally, in some cases, change in entropy upon binding is also considered in the calculations to improve the accuracy of the binding affinity predictions. MM-GBSA method is significantly faster than FEP (free energy perturbation) calculations, however it suffer from larger uncertainties than FEP, but in most cases is able to predict relative binding affinities in reasonable agreement with experimental data [23].

4.2.Chemistry

Commercially available reagents and solvents were used for the synthetic purpose. Pre-coated TLC plates were used to monitor the reactions. Column chromatography was carried out on silica gel 60-120 mesh for the purification and separation of compounds using a combination of ethyl acetate and petroleum ether. Melting points were obtained in open capillary tubes on a melting point apparatus. The IR spectra of the molecules were recorded on a FT-IR spectrophotometer, using KBr pellet. ^{1}H NMR and ^{13}C NMR spectra of the molecules were generated on a Bruker spectrophotometer at 400MHz and 100MHz (TMS as internal standard), respectively using $CDCl_3$ or DMSO as solvent. Mass spectra were also recorded on Waters Q-TOF micro ESI-MS spectrometer at positive ionization mode (ESI^+). The MS peaks were recorded as *m/z* ratio.

4.2.1. Synthesis of variedly substituted benzyl-1H-indole-3-carbaldehyde (3a-i).

A mixture of indole-3-carbaldehyde (**1)** (0.35 g, 2.5 mmol) and potassium carbonate (5 mmol) in acetone (10 ml) was stirred for 5 minutes. Next, variedly substituted benzyl chlorides (**2a-i)** (2.5 mmol) were added into the reaction mixture and stirred at 50°C. Completion of reaction was monitored by TLC. After completion of reaction, the mixture

was filtered to remove K_2CO_3 and concentrated under vacuum. Obtained crude product was dried and recrystallized with diethyl ether to afford the pure product (**3a-i)**.

4.2.2. Synthesis of variedly substituted (E)-3-(1-benzyl-1H-indol-3-yl)-1-(4-bromophenyl)prop-2-en-1-one (5a-i)

To a solution of N-substituted indole-3-carbaldehyde, **3a-i** (0.23 g, 10 mmol) and 4'-bromoacetophenone (**4)** (0.2 g, 10 mmol) in methanol (10 ml), few drops of piperidine were added. The reaction mixture was stirred for 2 h at 50°C and then left overnight in refrigerator. The reaction mixture was neutralized with diluted hydrochloric acid (1:1) and the solid formed was filtered off, washed with water, air dried and recrystallized from absolute ethanol. (**5a-i)**.

4.2.3. Synthesis of final compounds of Series I (7a-i).

A mixture of chalcones, **5a-i** (0.1 g, 0.25 mmol) and guanidine hydrochloride, **6** (0.25 mmol) solution in methanol (10 ml) containing sodium hydroxide (0.25 mmol) was stirred at 50°C for 6-8 h. After cooling, the reaction mixture was poured onto ice-water (50 mL) and the solid formed was filtered off, air dried to obtain the crude products (**7a-i)** which were purified by column chromatography (Silica gel # 60-120; Petroleum Ether: Ethyl acetate::80: 20).

4-(4-Bromophenyl)-6-(1-(4-ethylbenzyl)-1H-indol-3-yl)pyrimidin-2-amine **(7a)** light yellow solid, Yield: 33.5%, mp: 112-114^{o}C, R_f 0.51, IR (ν cm-1) 3307 (-NH_2), 1660 (C=N), 1632 (C=N), 1590 (C=N), 872 (C-Br); ^{1}H NMR (400 MHz, $CDCl_3$) δ (ppm): 8.23 (s, *NH_2*), 8.03-8.01 (d, *J* = 8 Hz, 1H), 7.99-7.96 (m, 1H), 7.92-7.89 (m, 1H), 7.72 (s, 1H), 7.66-7.64 (d, *J* = 8 Hz, 1H), 7.61-7.59 (m, 1H), 7.48-7.46 (m, 2H), 7.35-7.33 (m, 1H), 7.25 (s, 1H), 7.15-7.06 (m, 4H), 5.33 (s, 2H), 2.68 (m, 2H), 1.27 (m, 3H); ^{13}C NMR (100 MHz, $CDCl_3$) 163.55, 163.09, 158.82, 134.45, 134.97, 132.96, 131.94, 130.67, 129.38, 129.10, 128.80, 128.60, 128.50, 127.14, 126.16, 106.95, 55.53, 25.68, 15.55; MS (+ESI): *m/z* 483.10 $(M+H)^+$, 485.10 $(M+2+H)^+$. Anal. Calcd for ($C_{27}H_{23}BrN_4$): C, 67.08; H, 4.80; N, 11.59; Found C, 67.21; H, 4.77; N, 11.61.

4-(4-Bromophenyl)-6-(1-(4-(tert-butyl)benzyl)-1H-indol-3-yl)pyrimidin-2-amine **(7b)** Light Yellow solid, yield: 35.6%, mp: 110-112^{o}C, R_f 0.45, IR (ν cm-1) 3399 (-NH_2), 1637 (C=N), 1612 (C=N), 1572 (C=N), 872 (C-Br); ^{1}H NMR (400 MHz, $CDCl_3$) δ (ppm): 8.40-7.38 (m, 1H), 7.89-7.86 (m, 2H), 7.57-7.55 (d, *J* = 8Hz, 2H), 7.31-7.23 (m, 6H), 7.08-7.06 (m, 3H), 5.21 (s, 2H), 1.25 (s, 9H); ^{13}C NMR (100 MHz, $CDCl_3$) δ (ppm): 163.88, 163.56, 158.55, 137.56, 137.02, 133.51, 132.31, 131.89, 130.56, 128.72, 128.69, 127.13, 127.00, 126.95, 126.76, 125.99, 125.84, 124.66, 124.13, 118.63, 110.23, 53.54, 31.35; MS (+ESI): *m/z* 511.14 $(M+H)^+$, 513.13 $(M+2+H)^+$. Anal. Calcd for ($C_{29}H_{27}BrN_4$): C, 68.10; H, 5.32; N, 10.95; Found C, 68.23; H, 5.29; N, 10.98.

4-(4-Bromophenyl)-6-(1-(4-isopropylbenzyl)-1H-indol-3-yl)pyrimidin-2-amine **(7c)** light yellow solid, yield: 30.15%, mp: 125-127^{o}C, R_f 0.48, IR (ν cm-1) 3349 (-NH_2), 1644 (C=N), 1574 (C=N), 1511 (C=N), 871 (C-Br); ^{1}H NMR (400 MHz, $CDCl_3$) δ (ppm) 8.33-8.30 (m, 1H), 7.90-7.88 (m, 2H), 7.70 (s, 1H), 7.59-7.57 (d, *J* = 8 Hz, 2H), 7.36-7.34 (d, *J* = 8Hz, 2H), 7.32-7.29 (m, 2H), 7.20-7.14 (m, 2H), 7.10-7.08 (d, *J* = 8Hz, 2H) 5.23 (s, 2H), 2.89 (m, 1H), 1.25 (m, 6H); ^{13}C NMR (100 MHz, $CDCl_3$) δ (ppm) 163.85, 163.55, 163.48, 149.25, 148.77, 138.59, 137.54, 136.99, 133.80, 132.61, 131.88, 130.66, 127.40, 127.20, 126.26, 125.52, 124.66, 124.13, 121.77, 121.45, 116.96, 115.42, 110.82, 50.67, 33.84, 23.96; MS (+ESI): *m/z* 497.12 $(M+H)^+$, 499.12 $(M+2+H)^+$. Anal. Calcd for ($C_{28}H_{25}BrN_4$): C, 67.61; H, 5.07; N, 11.26; Found C, 67.74; H, 5.04; N, 11.29.

4-(4-Bromophenyl)-6-(1-(3-(trifluoromethyl)benzyl)-1H-indol-3-yl)pyrimidin-2-amine **(7d)** light yellow solid, yield: 25.6%, mp: 117-119^{o}C, R_f 0.48, IR (ν cm-1) 3309 (-NH_2), 1644 (C=N), 1574 (C=N), 1564 (C=N), 812 (C-Br); ^{1}H NMR (400 MHz, $CDCl_3$) δ (ppm): 8.40-8.38 (m, 1H), 7.91-7.89 (d, *J* = 8 Hz, 2H), 7.72 (s, 1H), 7.62-7.60 (d, *J* = 8 Hz, 2H), 7.54-7.50 (m, 2H), 7.42-7.38 (m, 2H), 7.32-7.23 (m, 4H), 5.40 (s, 2H); ^{13}C NMR (100 MHz, $CDCl_3$) 164.13, 163.41, 163.20, 138.25, 137.54, 136.79, 131.92, 131.81, 131.48, 130.09, 129.92,

128.70, 126.27, 125.53, 125.20, 124.80, 124.47, 123.84, 122.49, 121.81, 121.74, 116.70, 115.56, 110.15, 50.13; MS (+ESI): *m/z* 523.06 $(M+H)^+$, 525.06 $(M+2+H)^+$. Anal. Calcd for ($C_{26}H_{18}BrF_3N_4$): C, 59.67; H, 3.47; N, 10.71; Found C, 59.61; H, 3.46; N, 10.78.

4-(4-Bromophenyl)-6-(1-(4-methylbenzyl)-1H-indol-3-yl)pyrimidin-2-amine **(7e)** light yellow solid, yield: 25.8%, mp: 120-122^{o}C, R_f 0.42, IR (ν cm-1) 3369 (-NH_2), 1648 (C=N), 1590 (C=N), 1577 (C=N), 872 (C-Br); ^{1}H NMR (400 MHz, $CDCl_3$) δ (ppm): 8.43-8.41 (d, *J* = 8 Hz, 1H), 7.91-7.89 (m, 2H), 7.64-7.60 (t, *J* = 8 Hz, 2H), 7.51 (s, 1H), 7.37-7.34 (m, 2H) 7.31-7.27 (m, 2H), 7.15-7.11 (m, 2H), 7.08-7.05 (m, 2H), 5.34 (s, 2H), 5.07 (s, *NH_2*) 2.32 (s, 3H); ^{13}C NMR (100 MHz, $CDCl_3$) 163.82, 163.44, 139.23, 137.84, 137.51, 137.09, 134.07, 133.34, 132.78, 131.85, 130.44, 129.85, 129.60, 128.58, 127.10, 126.98, 124.58, 121.82, 116.38, 115.47, 110.41, 103.62, 50.40, 21.11; MS (+ESI): *m/z* 469.09 $(M+H)^+$, 471.09 $(M+2+H)^+$. Anal. Calcd for ($C_{26}H_{21}BrN_4$): C, 66.53; H, 4.51; N, 11.94; Found C, 66.67; H, 4.48; N, 11.96.

4-(4-Bromophenyl)-6-(1-(4-fluorobenzyl)-1H-indol-3-yl)pyrimidin-2-amine **(7f)** yellow solid, yield: 37.8%, mp: 115-117^{o}C, R_f 0.48, IR (ν cm-1) 3369 (-NH_2), 1648 (C=N), 1581 (C=N), 1511 (C=N), 812 (C-Br); ^{1}H NMR (400 MHz, $CDCl_3$) δ (ppm): 8.42-8.40 (dd, J_{13} = 6.8 Hz J_{12} = 1.6 Hz, 1H), 7.94-7.91 (m, 3H), 7.62-7.60 (d, *J* = 8 Hz, 2H), 7.38 (s, 1H), 7.32-7.28 (m, 3H), 7.16-7.12 (m, 2H), 7.02-6.98 (m, 2H), 5.35 (s, 2H), 5.11 (s, *NH_2*); ^{13}C NMR (100 MHz, $CDCl_3$) δ (ppm) 163.97, 163.47, 163.42, 137.37, 137.00, 132.19, 132.15, 131.89, 130.27, 128.69, 128.61, 126.29, 124.67, 122.93, 121.83, 121.56, 116.03, 115.82, 114.97, 110.30, 103.67, 49.91; MS (+ESI): *m/z* 473.06 $(M+H)^+$, 475.06 $(M+2+H)^+$. Anal. Calcd for ($C_{25}H_{18}BrFN_4$): C, 63.44; H, 3.83; N, 11.84; Found C, 63.69; H, 3.82; N, 11.88.

4-(4-Bromophenyl)-6-(1-(4-chlorobenzyl)-1H-indol-3-yl)pyrimidin-2-amine **(7g)** yellow solid, yield: 24.6%, mp: 113-115^{o}C, R_f 0.41; IR (ν cm-1) 3354 (-NH_2), 1654 (C=N), 1568

(C=N), 1531 (C=N), 852 (C-Br); ^{1}H NMR (400 MHz, $CDCl_3$) δ (ppm): 8.40-8.38 (d, *J* = 8Hz, 1H), 7.89-7.86 (m, 3H), 7.58-7.56 (d, *J* = 8Hz, 2H), 7.33 (s, 1H), 7.26-7.17 (m, 5H), 7.03-7.01 (d, *J* = 8Hz, 2H), 5.35 (s, NH_2), 5.25 (s, 2H); ^{13}C NMR (100 MHz, $CDCl_3$) δ (ppm): 163.88, 163.48, 163.28, 137.25, 136.88, 134.89, 133.76, 131.81, 130.34, 129.24, 129.05, 128.87, 128.69, 128.57, 128.17, 128.11, 126.22, 124.22, 121.79, 121.54, 114.91, 110.26, 103.56, 49.82; MS (+ESI): *m/z* 491.03 $(M+H)^+$, 493.03 $(M+2+H)^+$. Anal. Calcd for ($C_{25}H_{18}BrClN_4$): C, 61.30; H, 3.70; N, 11.44; Found C, 61.41; H, 3.68; N, 11.46.

4-(4-Bromophenyl)-6-(1-(3-chlorobenzyl)-1H-indol-3-yl)pyrimidin-2-amine (7h) Yellow solid, yield: 35.2%, mp: 120-122^{o}C, R_f 0.44, IR (ν cm-1) 3368 (-NH_2), 1653 (C=N), 1562 (C=N), 952 (C-Cl); ^{1}H NMR (400 MHz, $CDCl_3$) δ (ppm): 8.68-8.66 (m, 1H), 8.46 (s, 1H), 7.65-7.63 (d, *J* = 8 Hz, 2H), 7.55 (s, 1H), 7.47-7.44 (m, 1H), 7.34-7.26 (m, 4H), 7.24-7.18 (m, 4H), 5.50 (s, 2H); ^{13}C NMR (100 MHz, $CDCl_3$) δ (ppm): 163.82, 162.44, 140.07, 137.37, 137.20, 134.06, 132.03, 131.71, 130.64, 128.95, 127.93, 127.18, 126.54, 125.80, 123.22, 122.77, 121.24, 114.54, 110.61, 101.77, 47.24; MS (+ESI): *m/z* 491.03 $(M+H)^+$, 493.03 $(M+2+H)^+$. Anal. Calcd for ($C_{25}H_{18}BrClN_4$): C, 61.30; H, 3.70; N, 11.44; Found C, 61.45; H, 3.66; N, 11.44.

4-(4-Bromophenyl)-6-(1-(2-chlorobenzyl)-1H-indol-3-yl)pyrimidin-2-amine **(7i)** light yellow solid, yield: 32.5%, mp: 116-118^{o}C, R_f 0.48, IR (ν cm-1) 3342 (-NH_2), 1655 (C=N), 1571 (C=N), 1514 (C=N), 952 (C-Cl); ^{1}H NMR (400 MHz, $CDCl_3$) δ (ppm): 8.70-8.68 (m, 1H), 8.42 (s, 1H), 7.65-7.63 (d, *J* = 8 Hz, 2H), 7.54 (s, 1H), 7.49-7.47 (m, 1H), 7.34-7.26 (m, 4H), 7.24-7.18 (m, 4H), 5.59 (s, 2H); ^{13}C NMR (100 MHz, $CDCl_3$) 163.78, 163.16, 162.10, 136.91, 136.88, 134.42, 131.71, 131.22, 129.32, 129.09, 128.47, 128.20, 127.28, 125.98, 123.52, 122.80, 120.78, 114.17, 110.03, 101.20, 47.74; MS (+ESI): *m/z* 491.03 $(M+H)^+$, 493.03 $(M+2+H)^+$. Anal. Calcd for ($C_{25}H_{18}BrClN_4$): C, 61.30; H, 3.70; N, 11.44; Found C, 61.39; H, 3.73; N, 11.43.

4.3.*In-vitro* evaluation

In-vitro evaluation of inhibitory potential of the synthesized compounds was performed against EGFR (L858R), EGFR (T790M) and c-MET, using Z-LYTE® kinase assay. The Z´-LYTE® biochemical assay employs a fluorescence-based, coupled-enzyme format and is based on the differential sensitivity of phosphorylated and non-phosphorylated peptides to proteolytic cleavage. The peptide substrate is labelled with two fluorophores—one at each end—that make up a FRET pair. A ratio metric method, which calculates the ratio (the Emission Ratio) of donor emission to acceptor emission after excitation of the donor fluorophore at 400 nm, is used to quantitate reaction progress. A significant benefit of this ratio metric method for quantitating reaction progress is the elimination of well-to-well variations in FRET-peptide concentration and signal intensities.

In brief, for EGFR (L858R) inhibitory activity, Z'-LYTE™ Kinase Assay Kit - Tyrosine 4 Peptide (PV3193) was utilized. The 2X EGFR (ErbB1) L858R / Tyr 04 mixture was prepared in 50 mM HEPES pH 7.5, 0.01% BRIJ-35, 10 mM $MgCl_2$, 4 mM $MnCl_2$, 1 mM EGTA, 2 mM DTT. The final 10 µL Kinase Reaction consists of 0.2 - 1.68 ng EGFR (ErbB1) L858R and 2 µM Tyr 04 in 50 mM HEPES pH 7.5, 0.01% BRIJ-35, 10 mM $MgCl_2$, 2 mM $MnCl_2$, 1 mM EGTA, 1 mM DTT. After the 1 hour Kinase Reaction incubation, 5 µL of a 1:64 dilution of Development Reagent B was added, mixed in the assay plate and incubated the 15-µL development reaction for 1 hour at room temperature. Afterwards, the kinase reaction was stopped by adding 5 µL of Stop reagent. Finally, the fluorescence signals were measured at 445 nm and 520 nm for both donor and acceptor emission, respectively, to calculate the emission ratio.

For EGFR (T790M) inhibitory activity, Z'-LYTE™ Kinase Assay Kit - Tyrosine 4 Peptide (PV3193) was utilized. The 2X EGFR (ErbB1) T790M / Tyr 04 mixture was prepared in 50 mM HEPES pH 6.5, 0.01% BRIJ-35, 10 mM $MgCl_2$, 1 mM EGTA, 0.02% NaN_3. The final 10 µL Kinase Reaction consists of 3.9 - 39.3 ng EGFR (ErbB1) T790M and 2 µM Tyr 04 in 50 mM HEPES pH 7.0, 0.01% BRIJ-35, 10 mM $MgCl_2$, 1 mM EGTA, 0.01% NaN_3. After the 1 hour Kinase Reaction incubation, 5 µL of a 1:64 dilution of Development Reagent B was added, mixed in the assay plate and incubated the 15-µL development reaction for 1 hour at room temperature. Afterwards, the kinase reaction was stopped by adding 5 µL of Stop reagent. Finally, the fluorescence signals were measured at 445 nm and 520 nm for both donor and acceptor emission, respectively, to calculate the emission ratio.

For c-MET inhibitory activity, Z'-LYTE™ Kinase Assay Kit - Tyrosine 6 Peptide (PV4122) was utilized. The 2X MET (cMet) / Tyr 06 mixture was prepared in 50 mM HEPES pH 7.5, 0.01% BRIJ-35, 10 mM $MgCl_2$, 1 mM EGTA. The final 10 µL Kinase Reaction consists of 0.49 - 11.2 ng MET (cMet) and 2 µM Tyr 06 in 50 mM HEPES pH 7.5, 0.01% BRIJ-35, 10 mM $MgCl_2$, 1 mM EGTA. After the 1 hour Kinase Reaction incubation, 5 µL of a 1:128 dilution of Development Reagent A was added, mixed in the assay plate and incubated the 15-µL development reaction for 1 hour at room temperature. Afterwards, the kinase reaction was stopped by adding 5 µL of Stop reagent. Finally, the fluorescence signals were measured at 445 nm and 520 nm for both donor and acceptor emission, respectively, to calculate the emission ratio.

Calculate Emission Ratio

The Emission Ratio for each well on the assay plate was calculated by dividing the coumarin emission signal (445 nm) by the fluorescein emission signal (520 nm).

$$Emission\ Ratio = \ Coumarin\ Emission\ (445\ nm) / \ Fluorescein\ Emission\ (520\ nm)$$

Calculate Percent Phosphorylation

The extent of phosphorylation of each sample well (containing kinase) was determined according to the 0% and 100% Phosphorylation Control wells. There is a non-linear relationship between Emission Ratio and Phosphorylation, which the following equation accounts for:

$$\%\ Phosphorylation = 1 - [\frac{\{(Emission\ Ratio\ x\ F100\%) - \ C100\%\}}{\{(C0\% - \ C100\%) + \ [Emission\ Ratio\ x\ (F100\% - \ F0\%)]\}}]$$

Where:

$C_{100\%}$ = Average Coumarin emission signal of the 100% Phos. Control

$C_{0\%}$ = Average Coumarin emission signal of the 0% Phos. Control

$F_{100\%}$ = Average Fluorescein emission signal of the 100% Phos. Control

$F_{0\%}$ = Average Fluorescein emission signal of the 0% Phos. Control

Conflict of interest

Authors declare no conflict of interest.

Acknowledgement

This work was supported by the DBT under grant no. BT/PR8275/BID/7/455/2013.

References

[1] P.A. Jänne, J.C.-H. Yang, D.-W. Kim, D. Planchard, Y. Ohe, S.S. Ramalingam, M.-J. Ahn, S.-W. Kim, W.-C. Su, L. Horn, AZD9291 in EGFR inhibitor–resistant non–small-cell lung cancer, New England Journal of Medicine 372(18) (2015) 1689-1699.
[2] T.G. Bivona, R.C. Doebele, A framework for understanding and targeting residual disease in oncogene-driven solid cancers, Nature medicine 22(5) (2016) 472.
[3] P.K. Singh, H. Singh, O. Silakari, Kinases inhibitors in lung cancer: From benchside to bedside, Biochimica et Biophysica Acta (BBA)-Reviews on Cancer 1866(1) (2016) 128-140.
[4] P.K. Singh, O. Silakari, chemotherapeutics-resistance "arms" race: An update on mechanisms involved in resistance limiting Egfr inhibitors in lung cancer, Life sciences 186 (2017) 25-32.
[5] S. Kobayashi, T.J. Boggon, T. Dayaram, P.A. Jänne, O. Kocher, M. Meyerson, B.E. Johnson, M.J. Eck, D.G. Tenen, B. Halmos, EGFR mutation and resistance of non–small-cell lung cancer to gefitinib, New England Journal of Medicine 352(8) (2005) 786-792.
[6] C.-H. Yun, K.E. Mengwasser, A.V. Toms, M.S. Woo, H. Greulich, K.-K. Wong, M. Meyerson, M.J. Eck, The T790M mutation in EGFR kinase causes drug resistance by increasing the affinity for ATP, Proceedings of the National Academy of Sciences 105(6) (2008) 2070-2075.
[7] L. Capoferri, A. Lodola, S. Rivara, M. Mor, Quantum Mechanics/Molecular Mechanics Modeling of Covalent Addition between EGFR–Cysteine 797 and N-(4-Anilinoquinazolin-6-yl) Acrylamide, Journal of chemical information and modeling 55(3) (2015) 589-599.
[8] C. Carmi, A. Cavazzoni, S. Vezzosi, F. Bordi, F. Vacondio, C. Silva, S. Rivara, A. Lodola, R.R. Alfieri, S. La Monica, Novel irreversible epidermal growth factor receptor inhibitors by chemical modulation of the cysteine-trap portion, Journal of medicinal chemistry 53(5) (2010) 2038-2050.
[9] A. Tarozzi, C. Marchetti, B. Nicolini, M. D'Amico, N. Ticchi, L. Pruccoli, V. Tumiatti, E. Simoni, A. Lodola, M. Mor, Combined inhibition of the EGFR/AKT pathways by a novel conjugate of quinazoline with isothiocyanate, European journal of medicinal chemistry 117 (2016) 283-291.
[10] S. Butterworth, D.A. Cross, M.R.V. Finlay, R.A. Ward, M.J. Waring, The structure-guided discovery of osimertinib: the first US FDA approved mutant selective inhibitor of EGFR T790M, MedChemComm 8(5) (2017) 820-822.
[11] D. Callegari, K. Ranaghan, C. Woods, R. Minari, M. Tiseo, M. Mor, A. Mulholland, A. Lodola, L718Q mutant EGFR escapes covalent inhibition by stabilizing a non-reactive conformation of the lung cancer drug osimertinib, Chemical Science 9(10) (2018) 2740-2749.
[12] F. Cappuzzo, P. Jänne, M. Skokan, G. Finocchiaro, E. Rossi, C. Ligorio, P. Zucali, L. Terracciano, L. Toschi, M. Roncalli, MET increased gene copy number and primary resistance to gefitinib therapy in non-small-cell lung cancer patients, Annals of oncology 20(2) (2008) 298-304.
[13] S. Yano, T. Yamada, S. Takeuchi, K. Tachibana, Y. Minami, Y. Yatabe, T. Mitsudomi, H. Tanaka, T. Kimura, S. Kudoh, Hepatocyte growth factor expression in EGFR mutant lung cancer with intrinsic and acquired resistance to tyrosine kinase inhibitors in a Japanese cohort, Journal of thoracic oncology 6(12) (2011).
[14] Y. Li, F. Guessous, E.B. Johnson, C.G. Eberhart, X.-N. Li, Q. Shu, S. Fan, B. Lal, J. Laterra, D. Schiff, Functional and molecular interactions between the HGF/c-Met pathway and c-Myc in large-cell medulloblastoma, Laboratory investigation 88(2) (2008) 98.
[15] K.W. Robinson, A.B. Sandler, The role of MET receptor tyrosine kinase in non-small cell lung cancer and clinical development of targeted anti-MET agents, The oncologist 18(2) (2013) 115-122.
[16] E. Merkul, T. Oeser, T.J. Mueller, Consecutive Three-Component Synthesis of Ynones by Decarbonylative Sonogashira Coupling, Chemistry-A European Journal 15(20) (2009) 5006-5011.
[17] J.T. Vijay, N.K. Nagalingaiah, S.C. Nagarakere, G. Suresha, R.S. Kanchugarakoppal, M. Kempegowda, Concise synthesis of substituted meridianins, Cogent Chemistry 1(1) (2015) 1083068.

[18] E. El-Sawy, A. Mandour, K. Mahmoud, I. Islam, H. Abo-Salem, Synthesis, antimicrobial and anti-cancer activities of some new N-ethyl, N-benzyl and N-benzoyl-3-indolyl heterocycles, Acta Pharmaceutica 62(2) (2012) 157-179.
[19] P.K. Singh, O. Silakari, Novel EGFR (T790M)-cMET dual inhibitors: putative therapeutic agents for non-small-cell lung cancer, Future medicinal chemistry 9(5) (2017) 469-483.
[20] D.S. Biovia, Discovery studio modeling environment, San Diego: Dassault Systèmes (2015).
[21] R.A. Friesner, J.L. Banks, R.B. Murphy, T.A. Halgren, J.J. Klicic, D.T. Mainz, M.P. Repasky, E.H. Knoll, M. Shelley, J.K. Perry, Glide: a new approach for rapid, accurate docking and scoring. 1. Method and assessment of docking accuracy, Journal of medicinal chemistry 47(7) (2004) 1739-1749.
[22] S. Release, 1: Desmond Molecular Dynamics System, version 3.7, DE Shaw Research, New York, NY, Maestro-Desmond Interoperability Tools, version 3 (2014).
[23] M.D. Parenti, G. Rastelli, Advances and applications of binding affinity prediction methods in drug discovery, Biotechnology advances 30(1) (2012) 244-250.

Figure legends:

Fig. 1: RMSD plot of 7c in complex with EGFR (T790M) for the time period of 30 ns.

Fig. 2: RMSD plot of 7h in complex with cMET for the time period of 30 ns.

Fig. 3: 3D interaction diagram along with contact summary of 7c in complex with EGFR (T790M) after MD simulations of 30 ns.

Fig. 4: 3D interaction diagram along with contact summary of 7h in complex with cMET after MD simulations of 30 ns.

Scheme 1. Synthetic scheme of designed indole-pyrimidine analogues.

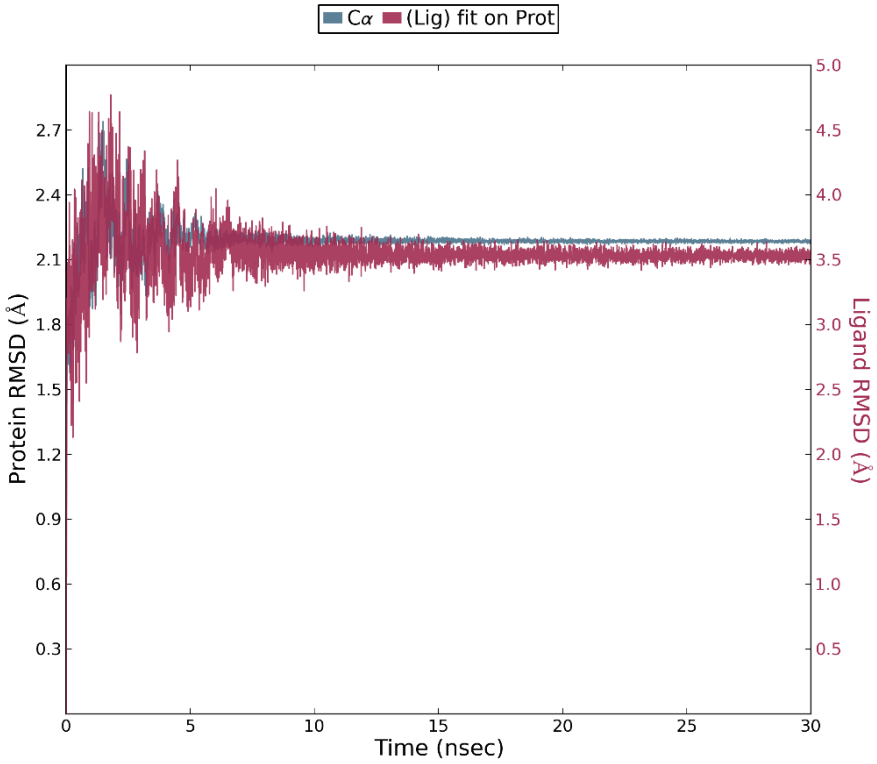

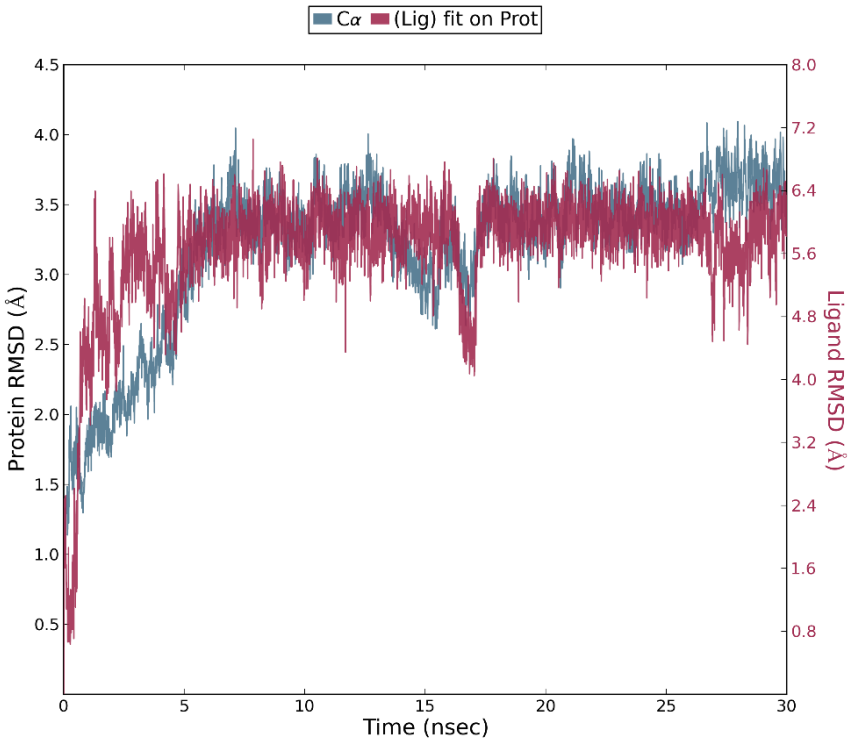

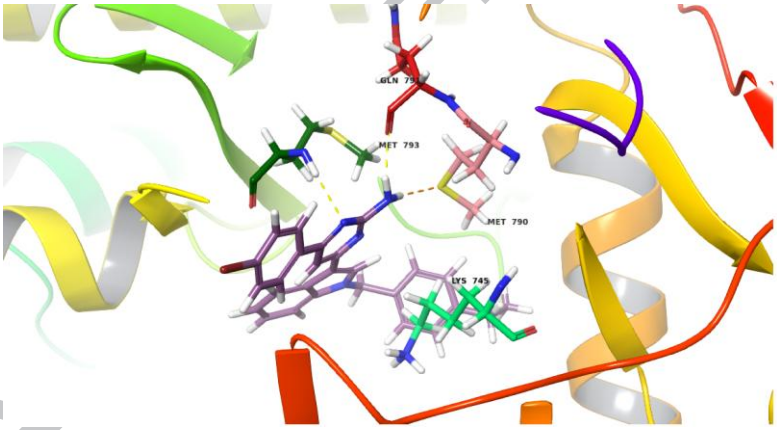

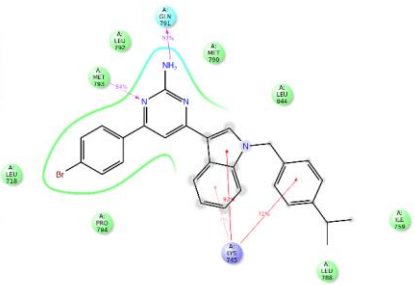

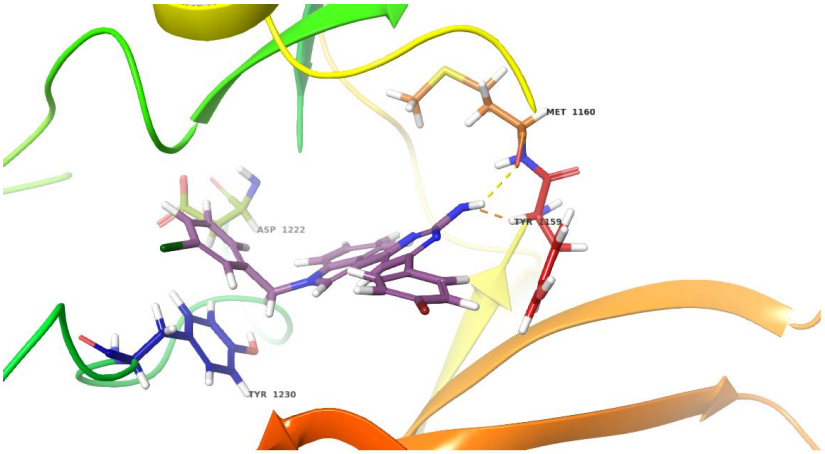

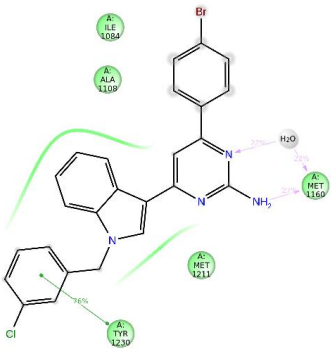

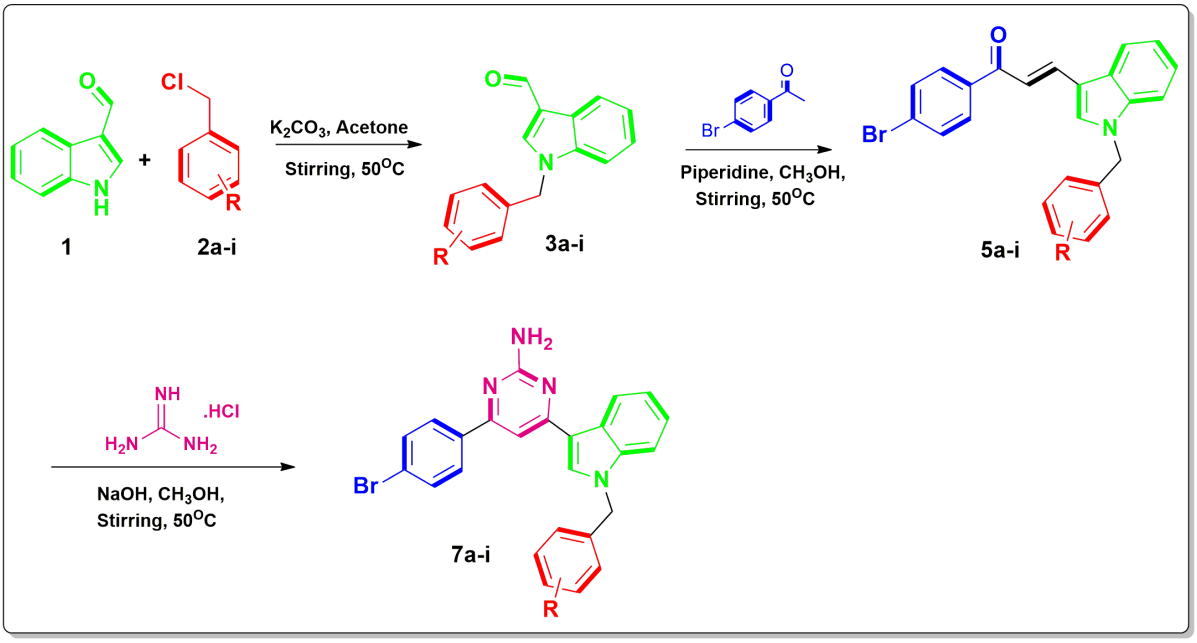

Table 1 Designed compounds with their binding energies and predicted activity.

S.No.	Compound	MM-GBSA binding energy (EGFR(T790M)	Predicted activity-EGFR(T790M) (µM)	MM-GBSA binding energy (cMET)	Predicted activity-cMET (µM)
1.	**7a**	-75.706	0.827	-79.450	0.124
2.	**7b**	-63.435	1.627	-68.614	0.128
3.	**7c**	-71.350	0.158	-66.319	0.115
4.	**7d**	-70.200	0.941	-73.562	0.123
5.	**7e**	-49.003	1.610	-81.705	0.135
6.	**7f**	-61.855	1.581	-81.573	0.126
7.	**7g**	-73.181	1.610	-68.174	0.137
8.	**7h**	-71.889	0.982	-84.334	0.124
9.	**7i**	-60.450	1.490	-82.288	0.125

Table 2. *In-vitro* kinase inhibitory data of designed compounds against EGFR (T790M), EGFR (L858R), cMET

S.NO.	Compound ID	R (subtituents)	EGFR (T790M) (µM)	EGFR (L858R) (µM)	cMET (µM)
1.	**7a**	**4-ethyl**	**0.097**	0.913	0.518
2.	7b	4-isobutyl	0.569	0.452	0.571
3.	**7c**	**4-isopropyl**	**0.094**	**0.099**	0.595
4.	7d	3-trifluoromethyl	0.494	0.998	0.293
5.	7e	4-methyl	0.757	0.866	0.588
6.	7f	4-fluoro	0.304	0.336	0.421
7.	7g	4-chloro	0.287	0.587	0.183
8.	**7h**	**3-chloro**	0.195	0.666	**0.101**

9.	7i	2-chloro	0.713	0.827	0.507
10.	Erlotinib	---------	0.907	0.032	------
11.	XL184	---------	--------	-------	0.030

Highlights:

- *In-silico* tools were used to identify scaffold with dual kinase inhibitory potential
- Focus was laid on hydrophobic interaction with mutant M790
- Molecules, also, having good binding affinity with cMET were selected
- *In-vitro* evaluation against EGFR (L858R), EGFR (T790M) and cMET was performed

Molecular dynamics guided development of indole based dual inhibitors of EGFR (T790M) and c-MET

Pankaj Kumar Singh, Om Silakari*

Molecular Modelling Lab (MML), Department of Pharmaceutical Sciences and Drug research,

Punjabi University, Patiala, Punjab, 147002, India

**Corresponding authors E-mail: omsilakari@gmail.com; Tel: +91-9501542696; Fax: +91-1752283075*

Graphical Abstract